Hindawi
Mobile Information Systems
Volume 2021, Article ID 5250778, 7 pages
https://doi.org/10.1155/2021/5250778

Research Article

Research on Networking Algorithm of Distributed FBG Sensor Network

Juan Wang,[1,2] Zhichao Liu,[1] Jinhua Yang,[1] and Zhentao Zhang[3]

[1]*School of Opto-Electronic Engineering, Changchun University of Science and Technology, Jilin 130022, China*
[2]*Jilin Vocational College of Industry and Technology, Jilin 132000, China*
[3]*College of Information and Control Engineering, Jilin Institute of Chemical Technology, Jilin 132000, China*

Correspondence should be addressed to Jinhua Yang; yangjh@cust.edu.cn

Received 13 August 2021; Revised 14 September 2021; Accepted 23 September 2021; Published 11 October 2021

Academic Editor: Sang-Bing Tsai

The status monitoring of industrial process equipment is of great significance to its production energy efficiency and safety. A state monitoring system for complex surface structures based on the distributed FBG sensor network is proposed. The system adopts the FBG network and realizes the calculation of the stress field of the complex surface through the FBG layout design at different positions in the three-dimensional space. A 32-channel FBG sensor network is designed, and the light source, demodulation module, and processing system are selected and analyzed. On the basis of building the FBG sensor network, the stress field test was carried out on the industrial process equipment. For complex three-dimensional surface structures, an optical scanner is used for position offset calibration. Experiments show that when force is applied to the center point, the slope of the FBG at the best sensitive position is 0.715 pm/N; when force is applied on both sides, the maximum slope in the positive direction is 0.348 pm/N and the maximum slope in the negative direction is −0.381 pm/N. After data fusion correction is used, the average error of the three-dimensional position offset of the test data is 6.85%. It can be seen that the FBG network has the ability to monitor the state of complex surface structures in the industrial engineering equipment.

1. Introduction

Fiber Bragg grating (FBG) sensors can write different gratings at any different positions on the same fiber, or cascade multiple gratings together, and then form a sensor array [1]. This feature is unique to fiber grating sensors and is an important way to build a large-capacity fiber grating sensor network to realize distributed sensing measurement. In recent years, the application of large-scale sensor networks composed of fiber grating sensors in the fields of building structural health monitoring, industrial safety production, environmental monitoring, photochemical biosensing, and smart materials has received extensive attention [2–4].

Liu et al. used the coded fiber grating sensor to construct a large-capacity distributed fiber grating sensor network and used the genetic tracking algorithm to improve the measurement accuracy [5]. Zhang et al. proposed a serial structure of ultraweak fiber Bragg gratings, using time-division multiplexing technology to increase the single-fiber FBG multiplexing by two orders of magnitude, which is of great significance for large-scale applications [6]. Ou et al. proposed a large-capacity weak fiber Bragg grating sensor array based on frequency shift interference technology, which greatly suppresses the crosstalk between FBGs and ensures the signal-to-noise ratio in the data acquisition process [7]. Liu et al. designed an FBG network structure applied to the acquisition of the temperature field of the granary. The network data have relevance and can complete positioning and regional analysis [8].

Optical multiplexing technology is an important technical means for constructing an FBG sensor network, and there are many kinds of optical multiplexing technology. The wavelength division multiplexing technology can set an independent working wavelength range for each FBG within the bandwidth of the light source [9]. This multiplexing

method makes the bandwidth of each FBG not overlap each other and avoids crosstalk. The reliability is high, but the bandwidth of the light source limits the number of sensors [10]. The space division multiplexing method allocates one transmission channel to each fiber grating. Its network layout is flexible, but its efficiency is low [11]. The above single multiplexing scheme may not meet the ideal requirements, so adopting a hybrid multiplexing scheme has higher universality.

This design uses a combination of wavelength division multiplexing and space division multiplexing to construct a sensor grating array. Each channel in the sensor array adopts wavelength division multiplexing in series with fiber gratings, and individual sensor gratings can be connected in series. The number depends on the scanning wavelength range of the system and the working wavelength range of each sensor grating, and space division multiplexing is used between different sensing channels to expand the capacity of the sensor grating.

2. Distributed Fiber Grating Sensor Network Design

Distributed FBG network is mainly composed of light source, F-P tunable filter [12], FBG array, receiving processing module, and data processing and control module. The structure diagram of n-channel FBG network is shown in Figure 1.

The signal light emitted by the light source enters the optical switch through the coupler, and the optical switch is controlled to realize the control of any channel. After the sensor channel is selected by the optical switch, the light reflected by the FBG is coupled to the tunable F-P filter by the 3 dB coupler. When the scanning wavelength of the F-P tunable filter is consistent with the resonant wavelength of a certain FBG, the light receiving device obtains the maximum light energy, thereby completing the identification. The F-P tunable filter is driven by the triangular wave scanning voltage generated by the optical switch drive device, and the transmitted light wavelength of the F-P tunable filter has a good linear relationship with the triangular wave scanning voltage value. When the physical quantity can change, the resonance peak to peak value and the resonance wavelength will change in the reflection spectrum. The mapping relationship between them is used to complete the inversion calculation of the physical quantity of the target position. The transmitted light signal of the tunable F-P filter is converted into an electrical signal by using a photoelectric sensor and then amplified and filtered into a pulse signal. The processing module performs data collection, calculation, and processing. Finally, the obtained signal is compared with the F-P etalon test data, so as to realize the effective demodulation of the signal.

2.1. Light Source Selection. When FBG is used as a sensing element, the selection of the light source is very critical. The light source is required to have both a higher output power and a higher signal-to-noise ratio. It can be seen that compared with the general broadband light source, the superluminescent diode has the characteristics of high output power, selectable center wavelength, wide spectral range, and good spectral flatness. Broadband light source is a superluminescent diode dedicated to special application fields such as optical fiber sensing and optical testing instruments [13]. The output power of this type of light source is adjustable within a certain range, and it is an ideal light source for a single grating sensing system. However, in a fiber grating sensing network with a larger multiplexing capacity, as the length of the fiber increases, if this type of broadband light source is used, the signal-to-noise ratio of the system will drop sharply, which limits the number of multiplexed fiber grating sensors and the application of the system in long-distance measurement [14]. It is particularly important to choose a high-power, stable, and reliable light source with multiwavelength output in a large-capacity FBG network. This system uses a tunable narrow-band light source based on a semiconductor optical amplifier as the light source of the sensor network. The spectral range of the light source is between 1530 and 1610 nm, and the minimum adjustable wavelength is 0.05 nm. An optical isolation unit is set for it to suppress the influence on the light source.

2.2. Tunable F-P Filter. There are two high-reflection mirrors in the F-P cavity, one of which is fixed and the other can be moved under the action of external force, and a piezoelectric ceramic is attached to the back of the mirror. Piezoelectric ceramics can be deformed under different voltages, so that the cavity length of the F-P cavity changes, and finally the wavelength of the light wave passing through the F-P cavity changes. When the wave peak of the light passing through the FP cavity coincides with the reflection wave peak of the sensor grating, the photoelectric detection device can detect the maximum light intensity. At this time, the scanning voltage value applied to the piezoelectric ceramic is the same as the reflection wavelength value of the sensor grating. This design changes the cavity length of the F-P cavity by applying a triangular wave scanning voltage to the piezoelectric ceramics and then changes the wavelength of the light transmitted by the F-P cavity. The F-P tunable filter is an important component of the fiber grating sensor network, and its measurement accuracy is directly related to the measurement accuracy of the entire sensor network.

In this design, the FOTF-CLII F-P filter of Oriental Spectroscopy Company is selected, the maximum scanning rate is 300 Hz, and the controllable wavelength range is 50–100 nm. The triangular wave scanning voltage of the F-P cavity is controlled by the optical switch controller, and the pulse width modulation (PWM) signal conversion is completed through FPGA.

2.3. Processing Module. After FPGA completes the grating channel selection and output, the F-P cavity is scanned after the 300 Hz triangular wave voltage signal is used, and the data acquisition is completed when the PIN diode obtains the maximum light intensity. The signal acquisition and processing are completed within one cycle of the triangular

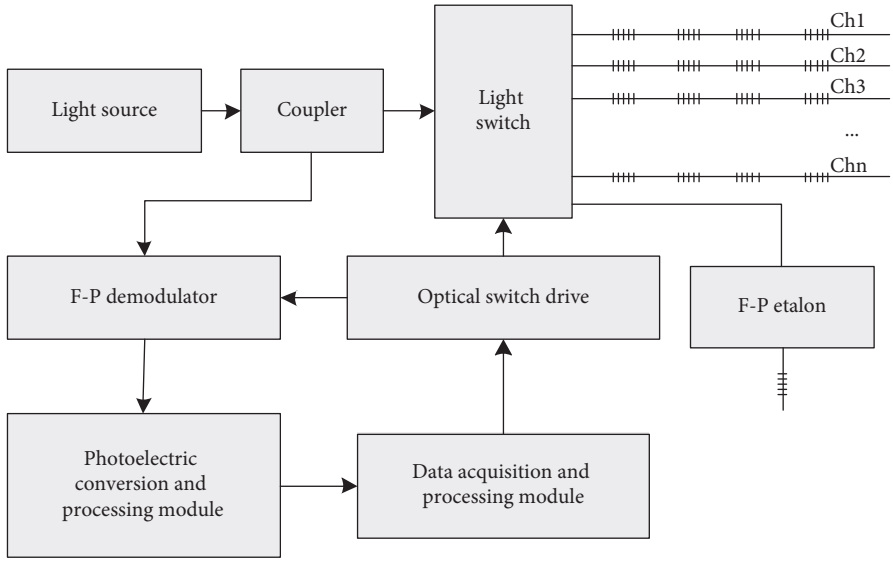

Figure 1: Distributed FBG network structure diagram of n channel.

wave. After sampling the information of the sensor grating of n channels, the data are stored and displayed until the program is exited. The program flow is shown in Figure 2. The n channel can simultaneously obtain the data of the FBG sensor group at different positions on the n optical fibers. The data scanning capability depends on the FBG demodulator and data acquisition card. As long as one set of test data can be effectively transmitted, the n channels only have certain requirements on the overall acquisition time of the system and have no effect on the test accuracy and test area settings.

3. FBG Network Data Fusion Algorithm

After the incident light enters the optical fiber, part of the light is reflected and part of the light is refracted. The light that meets the Bragg condition will be reflected, and the light that does not meet the condition will be projected [15]. The Bragg condition that must be met for reflected light is

$$\lambda_B = 2n_{\text{eff}}\Lambda, \tag{1}$$

where λ_B is the central wavelength of the fiber grating sensor, n_{eff} is the effective refractive index, and Λ is the grating period.

When the external environment temperature or stress changes, the effective refractive index changes accordingly, and it causes the center wavelength to shift. When temperature calibration is used, the wavelength shift corresponding to the stress can be expressed as

$$\frac{\Delta\lambda_B}{\lambda_B} = (1 - \mathrm{P}_e)\varepsilon, \tag{2}$$

where $\Delta\lambda_B$ is the offset of the center wavelength of the emitted light, P_ε is the effective elastic-optical coefficient, and ε is the axial strain.

First, establish the coordinate system O_D-$X_DY_DZ_D$ and O_Q-$X_QY_QZ_Q$ in the docking network. O_D represents the origin of the coordinate, X_D represents the X axis in the D coordinate system, Y_D represents the Y axis in the D coordinate system, and Z_D represents the Z axis in the D coordinate system. From the measurement data of the fiber grating sensor and the strain-displacement conversion relationship, the position of the moving part in the coordinate system O_D-$X_DY_DZ_D$ can be known, and the attitude adjustment reference is measured by the fiber grating measurement system. The point set of the point is Q_{PAi} in the global coordinate system, and the point set under the moving part is D_{PAi}. The singular value method is used to solve the rotation matrix R and the translation matrix T, so that the point set can be transferred from the mobile coordinate system to the global coordinate system. The two coordinate systems can be registered:

$$D_QP = \begin{bmatrix} D_QR & D_QT \\ 0 & 1 \end{bmatrix}, \tag{3}$$

where ${}^Q_DR \in R^{3\times3}$ is the rotation matrix transformed from the moving part coordinate system to the global coordinate system and ${}^Q_DT \in T^{3\times1}$ is the transformation from the moving coordinate system to the translation matrix of the global coordinate. The posture can be defined as

$$\Delta^{\mathrm{Q}}P_O = {}^{\mathrm{Q}}P_{O2} - {}^{\mathrm{Q}}P_{O1}. \tag{4}$$

After the point set is registered, the moving part can be moved from the current pose P_{v1} to the target pose P_{v2}. After obtaining the pose parameters of the moving part, the movement displacement matrix δ_1 and the rotation displacement matrix δ_2 of the part in the global docking process can be obtained. The calibration can get the position of the coordinate center of the movable platform in the global coordinate system as the vector ${}^{\mathrm{O}}P_{O1}$, and the position vector after the docking is ${}^{\mathrm{O}}P_{O2}$. Then, the global movement path is

$$\Delta^{\mathrm{Q}}P_O = {}^{\mathrm{Q}}P_{O2} - {}^{\mathrm{Q}}P_{O1}. \tag{5}$$

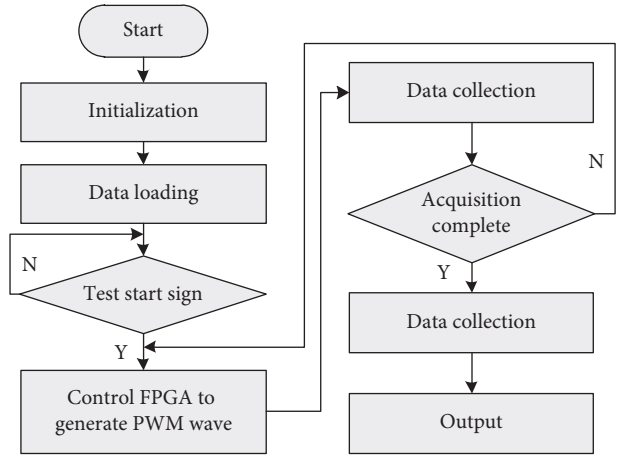

Figure 2: Flowchart of system process.

4. Experiment

4.1. Experimental Conditions. A three-dimensional strain field surface based on the FBG sensor is established, and the three-dimensional strain field detection network is applied to the electrical distribution structure. The process control system is shown in Figure 3. The system consists of the surface to be tested, FBG sensor (SNE-26 type), fiber grating demodulator (SA-II type, 1525–1565 nm, light source flatness ≦ 2 dBm), etc. During the curved surface stress test, an adjustable stress is used to load the test surface, the test range is 0–100 *N*, a set of data is recorded every 5.0 N, and the average of each set of data is collected 10 times.

As shown in Figure 3, the main test surface of the FBG sensor is a convex surface with continuous and gradual changes in the surface. Therefore, when testing the surface strain field, the characteristic positions of the strain field are mainly obtained at the center, left edge, and right edge of the structure. Because the test surface has certain symmetry, the strain field changes on both sides of the center can be obtained to get the strain distribution trend of other edge positions with the center point as the center. It can be seen that there are three main test positions in the test process. For the FBG sensor, the best sensitivity is its axial test capability. Therefore, using two perpendicularly crossing FBG sensors at the same position can completely obtain the stress field distribution at this location. It can be seen that the six FBG sensors used in the whole test can fully obtain the distribution characteristics of the strain field on the surface to be tested. When there are less than 6, the characteristic data are incomplete. When there are more than 6, although more test data can be obtained, the final characterization results are similar, which increases the complexity of the system.

In order to solve the temperature and strain cross-sensitivity of FBG sensors, this system adopts two sets of test FBG sensors. The temperature FBG sensor is used to calibrate the strain FBG sensor. First, fix the temperature FBG sensor on the structure to be tested and calculate the FBG wavelength offset after obtaining the real-time temperature test data. Then, the wavelength offset is compensated for the strain test FBG sensor. The packaging structure of the temperature FBG sensor adopts a steel cylinder. The stable structure makes it hardly affected by external stress, and the temperature is transferred to the temperature FBG sensor from the steel cylinder with good thermal conductivity.

4.2. FBG Networking Test. In order to better express the test effect, the FBG with six characteristic positions is used for comparative analysis. The change of microstrain ($\mu\varepsilon$) is observed at different positions of the workpiece under different pressures. FBG sensor reflection spectrum center wavelength deviation $\Delta\lambda_B$ is proportional to the microstrain ($\mu\varepsilon$) of the measured point. The test result is shown in Figure 4.

As can be seen from the test chart, when the pressure is loaded at different positions, the corresponding echo responses have obvious differences. As shown in Figure 4(a), the stress acts on the center position and the response of FBG1 becomes linear with a slope of 0.715 pm/N. The analysis believes that the sticking position of FBG1 is near the center point. The change slope of FBG2–FBG6 is between 0.156 pm/N and 0.216 pm/N. As shown in Figure 4(b), the stress acts on the left side of the structure to be tested. FBG3 and FBG5 change in a positive direction, with an average slope of 0.325 pm/N, while FBG2, FBG4, and FBG6 change in a negative direction, with an average slope of −0.281 pm/N. It is found that, under the condition of applying force on the left side, one side of the structure is in a compressed state and the other side is in a stretched state. As shown in Figure 4(c), the stress acts on the right side of the structure to be tested. FBG3 and FBG5 change in a negative direction, with an average slope of −0.381 pm/N, while FBG2, FBG4, and FBG6 change in a positive direction, with an average slope of 0.348 pm/N. It can be seen that the FBG network can well analyze the stress field distribution of the structure to be tested.

4.3. Data Fusion Analysis. The temperature data obtained by the test and the stress field data are merged, and they are unified to the surface change of the test structure to complete

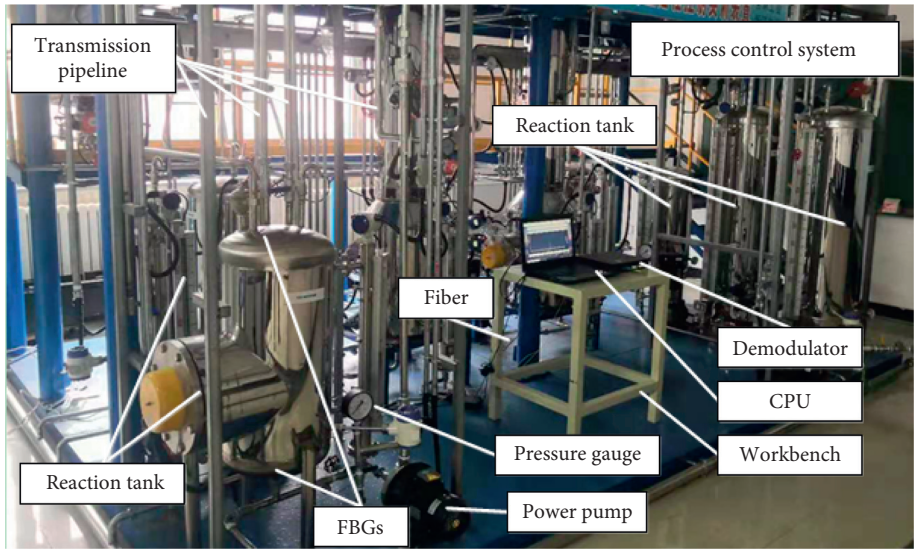

Figure 3: Physical distribution diagram of the experimental device.

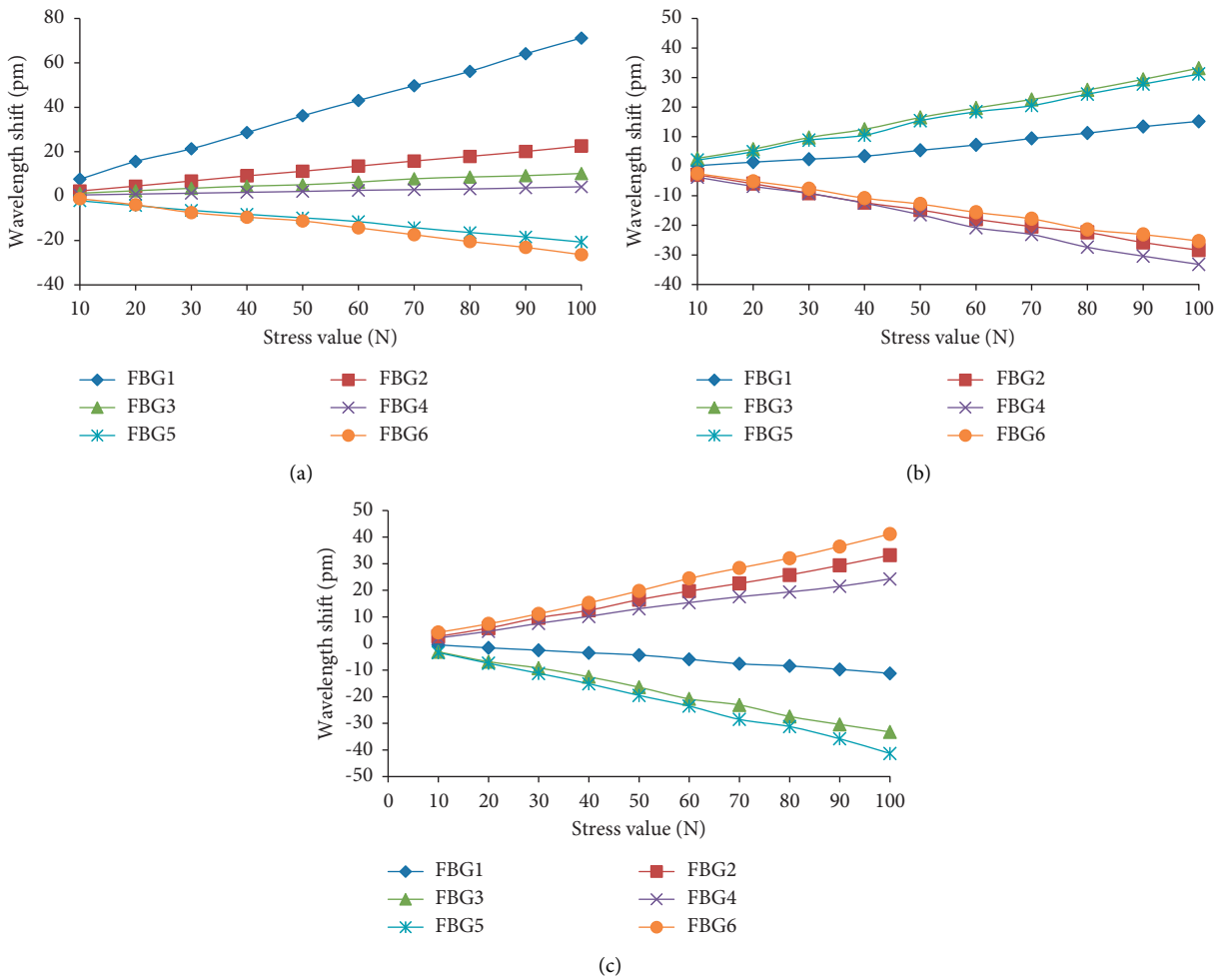

Figure 4: Schematic diagram of fiber wavelength offset. The pressure point is (a) in the middle, (b) on the left, and (c) on the right.

Table 1: Data fusion comparison relationship.

No.	Coordinates	FBG (mm)			Optical scanner (mm)	Error (%)
		Temperature	Strain	Fusion		
1	x	0.07	1.38	1.45	1.40	3.57
	y	0.07	−0.54	−0.47	−0.45	4.44
	z	0.06	−0.31	−0.25	−0.21	8.69
2	x	0.08	1.14	1.22	1.24	3.93
	y	0.07	0.42	0.49	0.47	4.25
	z	0.07	0.35	0.42	0.39	7.69
3	x	0.06	0.14	0.20	0.18	9.98
	y	0.05	−1.57	−1.52	−1.43	6.29
	z	0.06	−0.28	-0.22	−0.25	−8.33
4	x	0.07	0.67	0.74	0.81	−8.64
	y	0.05	−0.58	−0.53	−0.59	−8.62
	z	0.06	0.85	0.91	1.04	−8.08

the analysis of the degree of surface deviation. Take 4 points in the test structure and distribute them evenly on the entire surface, and then map the offset correction values of temperature and strain to the position deviation. Using the test data of the optical scanner as the standard value, the test results are shown in Table 1.

It can be seen from Table 1 that the use of FBG can analyze the three-dimensional position shift of the target structure, but there is a certain error compared with the optical scanning method. Through data fusion of temperature compensation and strain field test results, the fusion correction effect can be obtained. The maximum error between the corrected test data and the optical scanning test result is 9.98%, the minimum is 3.57%, and the average is 6.85%. Through data fusion, the test accuracy has been improved. It can be seen that the FBG sensor network proposed in this paper has a good detection effect in the testing of three-dimensional complex surface structures.

5. Conclusion

This paper designs a multi-FBG sensor network, which realizes the acquisition of structure state information through FBGs at different positions in the three-dimensional space. Under the condition of temperature calibration, the three-dimensional stress field can be calculated. At the same time, according to the calculation method in this paper, the test data of multiple FBGs can also be used to calculate the three-dimensional position offset of the structure. Finally, the feasibility of the system is verified through experiments, and the network has certain advantages in the condition monitoring of three-dimensional structures.

Data Availability

No data were used to support this study.

Ethical Approval

This article does not contain any studies with human participants performed by any of the authors.

Consent

There is no informed consent involved.

Conflicts of Interest

All authors declare that they have no conflicts of interest.

Authors' Contributions

Juan Wang performed editing. Zhichao Liu was involved in implementation of research process. Jinhua Yang was involved in data collection. Zhentao Zhang contributed to design and conception.

Acknowledgments

This work was supported by Scientific Research and Industry Department of Jilin Province (Visual Intelligent Perception Integrated Production Process Automatic Control System Based on 3D Reconstruction of Curvature Gradient Interpolation of Composite Fiber Array, No. JJKH20210220KJ), the National Science Foundation of China (Theoretical Model and Experimental Research on the Novel FBG Sensing System Based on the Fusion Algorithm, No. 61703056), and Jilin Province Science and Technology Development Plan Project (No. 20190103154JH).

References

[1] E. Mesquita, L. Pereira, A. Theodosiou et al., "Optical sensors for bond-slip characterization and monitoring of RC structures," *Sensors and Actuators A: Physical*, vol. 280, no. 1, pp. 332–339, 2018.

[2] J. Botsis, L. Humbert, and F. Colpo, "Embedded fiber Bragg grating sensor for internal strain measurement sin polymeric materials," *Optics and Laser sin Engineering*, vol. 43, no. 3, pp. 491–510, 2005.

[3] X. Ou, L. Shaohua, F. Suchun, and J. Shuisheng, "A novel fiber-laser-based fiber Bragg grating strain sensor with high-birefringence Sagnac fiber loop mirror," *Chinese Optics Letters*, vol. 6, no. 11, pp. 818–820, 2008.

[4] J. H. Osório, G. Chesini, and A. Valdir, "Serrão, Simplifying the design of microstructured optical fibre pressure sensors," *Scientific Reports*, vol. 7, no. 2990, pp. 372–381, 2017.
[5] H. Liu, C. Wang, and Y. Chen, "An improved genetic algorithm for increasing the addressing accuracy of encoding fiber Bragg grating sensor network," *Optical Fiber Technology*, vol. 40, pp. 28–35, 2018.
[6] S. Zhang, M. Chen, Q. He, W. Chen, H. Chen, and H. Li, "Quasidistributed fiber Bragg grating sensor network based on self-heterodyne detection technique," *Optical Engineering*, vol. 53, no. 5, Article ID 057107, 2014.
[7] Y. Ou, C. Zhou, and L. Qian, "Large-capacity multiplexing of Near-identical weak fiber Bragg gratings using frequency-shifted Internet [J]," *Optics Express*, vol. 23, no. 24, p. 3148, 2015.
[8] Z. C. Liu, J. H. Yang, and L. Zhang, "Granary temperature measurement network based on chirped FBG[J]," *Spectroscopy and Spectral Analysis*, vol. 10, no. 1, pp. 3377–3380, 2016.
[9] B. Sun, J. Li, and W. Zhang, "Fiber Bragg grating sensor," *Optical Fiber Sensing and Structural Health Monitoring Technology*, vol. 26, no. 4, pp. 77–148, 2019.
[10] Y. Kuang, L. Y. Guo, and W. Liu, "Packaging and temperature compensation of fiber Bragg grating for strain sensing: a survey," *Photonic Sensors*, vol. 8, no. 4, pp. 320–331, 2018.
[11] L. Sun, H. Hao, B. B. Zhang, and B. Ren, "Strain transfer analysis of embedded fiber Bragg grating strain sensor," *Journal of Testing and Evaluation*, vol. 44, no. 6, pp. 2312–2320, 2016.
[12] A. G. Leal-Junior, C. A. R. Díaz, F. Anselmo, M. Carlos, R. N. R. Moisés, and P. Maria José, "Simultaneous measurement of pressure and temperature with a single FBG embedded in a polymer diaphragm," *Optics & Laser Technology*, vol. 112, no. 193, pp. 77–84, 2019.
[13] Y. M. Al-Anany and M. J. Tait, "Fiber-reinforced elastomeric isolators for the seismic isolation of bridges," *Composite Structures*, vol. 160, no. 7, pp. 300–311, 2016.
[14] M. Mulle, G. A. Yudhanto, and W. R. N. SchijveYaldiz, "Internal strain assessment using FBGs in a thermoplastic composite subjected to quasi-static indentation and low-velocity impact," *Composite Structures*, vol. 215, no. 32, pp. 305–316, 2019.
[15] C.-w. Verghese, S.-c. Lei, W.-s. Chen, and S.-r. Song, "Downhole fiber optic temperature-pressure innovative measuring system used in Sanshing geothermal test site," *Geothermics*, vol. 74, no. 31, pp. 190–196, 2018.